AD-A069 583 VIRGINIA POLYTECHNIC INST AND STATE UNIV BLACKSBURG D--ETC F/G 20/4
A MILLIMETER WAVE ATTENUATION AND DEPOLARIZATION EXPERIMENT USI--ETC(U)
APR 79 W L STUTZMAN, C W BOSTIAN DAAG29-77-G-0083
UNCLASSIFIED ARO-14066.4-EL NL

1 OF 1
AD A069583

END
DATE FILMED
7-79
DDC

A MILLIMETER WAVE ATTENUATION AND DEPOLARIZATION EXPERIMENT USING THE COMSTAR AND CTS SATELLITES

by

W. L. Stutzman and C. W. Bostian
Electrical Engineering Department
Virginia Polytechnic Institute and State University
Blacksburg, Virginia 24061

Prepared for

U.S. Army Research Office
P. O. Box 12211
Research Triangle Park, North Carolina 27709

Under

Project No. P14066-EL
Grant No. DAAG29-77-G-0083
Grant Period 1 May 1977 - 30 October 1978

In Conjunction With

Contract NAS5-22577
NASA Goddard Space Flight Center
Greenbelt, Maryland 20771

Approved for Public Release:
Distribution Unlimited

The findings in this report are not to be construed as an official Department of the Army position, unless so designated by other authorized documents.

(18) ARO, SATCOM (19) J4066.4-EL,79-2

Unclassified

SECURITY CLASSIFICATION OF THIS PAGE (When Data Entered)

REPORT DOCUMENTATION PAGE

READ INSTRUCTIONS BEFORE COMPLETING FORM

1. REPORT NUMBER

2. GOVT ACCESSION NO.

3. RECIPIENT'S CATALOG NUMBER

(9)

4. TITLE (and Subtitle)

(6) A Millimeter Wave Attenuation and Depolarization Experiment Using the COMSTAR and CTS Satellites.

5. TYPE OF REPORT & PERIOD COVERED
Final Report -
1 May 1977-30 Oct 1978

6. PERFORMING ORG. REPORT NUMBER
SATCOM-79-2

7. AUTHOR(s)

(10) Warren L. Stutzman
Charles W. Bostian

8. CONTRACT OR GRANT NUMBER(s)

(15) Grant No.
✓ DAAG29-77-G-0083
NAS5-22577

9. PERFORMING ORGANIZATION NAME AND ADDRESS
Virginia Polytechnic Institute & State Univ.
Department of Electrical Engineering
Blacksburg, Virginia 24061

10. PROGRAM ELEMENT, PROJECT, TASK AREA & WORK UNIT NUMBERS

11. CONTROLLING OFFICE NAME AND ADDRESS
U. S. Army Research Office
P. O. Box 12211
Research Triangle Park, NC 27709

(11) 15 Apr 1979

12. REPORT DATE

13. NUMBER OF PAGES
54

14. MONITORING AGENCY NAME & ADDRESS (If different from Controlling Office)

(12) 55p.

15. SECURITY CLASS. (of this report)
Unclassified

15a. DECLASSIFICATION/DOWNGRADING SCHEDULE

16. DISTRIBUTION STATEMENT (of this Report)

Approved for public release; distribution unlimited.

17. DISTRIBUTION STATEMENT (of the abstract entered in Block 20, if different from Report)

18. SUPPLEMENTARY NOTES
The view, opinions, and/or findings contained in this report are those of the author(s) and should not be construed as an official Department of the Army position, policy, or decision, unless so designated by other documentation.

19. KEY WORDS (Continue on reverse side if necessary and identify by block number)

synthetic storm models
COMSTAR satellites
CTS satellites
millimeter waves
communication links
rain attenuation models

20. ABSTRACT (Continue on reverse side if necessary and identify by block number)
This report provides the results of a study of attenuation and depolarization of millimeter waves along a satellite-to-earth communication link. Specifically, 1) Detailed analysis of attenuation and depolarization data from the CTS (Communications Technology Satellite) satellite downlink beacon at a frequency of 11.7 GHz, and the 19.04 and 28.56 GHz downlink beacons on the COMSTAR satellites, and 2) Development of physical models of rain attenuation and depolarization.

411062

DD FORM 1 JAN 73 1473 EDITION OF 1 NOV 65 IS OBSOLETE

Unclassified

SECURITY CLASSIFICATION OF THIS PAGE (When Data Entered)

FOREWARD

The goals of this research project, as detailed in the proposal, were to provide additional support for the study of attenuation and depolarization of millimeter waves along a satellite-to-earth communication link. Specifically, this support contributed to our research efforts in 1) Detailed analysis of attenuation and depolarization data from the CTS (Communications Technology Satellite) satellite downlink beacon at a frequency of 11.7 GHz, and the 19.04 and 28.56 GHz downlink beacons on the COMSTAR satellites, and 2) Development of physical models of rain attenuation and depolarization. These two activities are, of course, very closely related. It is necessary to have a reliable data base for the development of a theoretical model. On the other hand, data collected for a specific location frequency, polarization, and elevation angle cannot be extrapolated to other locations, frequencies, polarizations, and elevation angles with full confidence. Our approach is to build a model which accurately predicts propagation effects as verified by comparison to data for several locations, frequencies, polarizations and elevation angles, and then use the model to predict attenuation and depolarization for situations where no data exists but applications do. A reliable model eliminates the time and expense of experimental data collection in advance of an operational system. It is the aim of this research effort to construct such a data-confirmed theoretical model.

Since this research has received multiple agency support, documentation of the results is found in several sources. Very detailed reports on the data collected are found in [1]-[3]. Information on the experimental

hardware is found in [4]. Details on the data reduction procedure used are contained in [1].

Support from the U.S. Army permitted concentration of effort on an existing theoretical analysis effort in the form of a Rain Propagation Prediction (RPP) computer program. This program was used to develop a Synthetic Storm Model (SSM). The synthetic storm model provides data concerning the physical nature of the rain, such as the rain rate distribution, rain path extent, and rain drop canting angle distribution. This together with system parameter values (frequency, elevation angle, and antenna polarization) is used as input with the RPP program to generate predicted values of signal fade, isolation, and phase as a function of earth station rain rate. Details of this theoretical model development are found in [5].

In this report recent results and essential conclusions of the modeling investigation are presented. There are two major findings which are directly traceable to the theoretical effort support by the Army: the synthetic storm model and the nonreciprocal effects of rain on propagation. These two topics are discussed in this report.

TABLE OF CONTENTS

PART I

A SYNTHETIC STORM MODEL FOR PREDICTION OF MILLIMETER WAVE RAIN ATTENUATION

A. INTRODUCTION

Theoretical procedures for predicting millimeter wave attenuation introduced by rain usually require a uniform rain rate along the propagation path. However, nonuniform rain rate conditions frequently occur on earth-satellite paths. The total attenuation introduced by real (nonuniform) rain is of interest for communication system applications. The effective path length approach is a popular method for predicting total attenuation on a satellite path, but we will show that the effective path length formulation is inherently restrictive.

Total attenuation can be determined more directly by the synthetic storm model, which is introduced here. This model includes the nonuniform character of the rain in a way that facilitates prediction for various elevation angles and frequencies. Attenuation data from several experiments are presented in support of the model. Scaling of attenuation values from one frequency to another is discussed. Also, the synthetic storm model together with the Rice-Holmberg rain rate equation [6] is used to predict attenuation statistics from rainfall accumulation data.

B. THE EFFECTIVE PATH LENGTH MODEL

Many of the theoretical developments in rain attenuation prediction have centered on specific attenuation α, which is the signal attenuation caused by a uniform rain-filled space one kilometer in extent. Specific attenuation is a function of both the rain and system parameters and can be expressed by the power relation

$$\alpha(R,f,\varepsilon) = a_1 R^{b_1} \qquad \text{dB/km} \tag{1}$$

where R is the rain rate in mm/hr, f is the frequency, and ε is the elevation angle of the propagation path. Constants a_1 and b_1 are available from 1 to 1000 GHz [7]; however, in [7] they were derived assuming spherical raindrops. A more accurate drop shape distribution [5] uses a mixture of oblate spheroidal and spherical raindrop shapes. Although not shown explicitly in (1), α is a function of the fraction of oblate drops as well as the polarization state of the incident wave and the orientation of the electric field relative to the canting angles of the oblate drops. The parameter dependences of α must be considered when developing a total attenuation model and particularly when a power law fit is employed.

The total attenuation due to a rain of physical extent L along the propagation path is given by

$$A(f,\varepsilon) = \int_0^L \alpha\{R(\ell),f,\varepsilon\}\, d\ell \qquad \text{dB} \tag{2}$$

where ℓ is the position along the rain portion of the path. Usually the rain rate as a function of position is not known, therefore, (2) is not evaluated directly. Instead, the effective path length model is used

frequently. Effective path length is defined as

$$L_e(R_{av},f,\varepsilon) = \frac{A}{\alpha} \qquad \text{km} \qquad (3)$$

where the average rain rate is given by

$$R_{av} = \frac{1}{L} \int_0^L R(\ell)\, d\ell \qquad \text{mm/hr} . \qquad (4)$$

The effective path length is obtained from (3) using experimental values of total attenuation A and theoretical values of specific attenuation α, and matching values of attenuation and rain rate observed for equal percentages of time. Typical effective path length values are shown in Fig. 1. These data were collected at VPI&SU along the nearly same rain paths. [2] The 19.04 GHz data is for the calendar year 1978 and is a combination of measurements taken with the COMSTAR D-2 and D-3 satellite beacons at elevation angles of 44° and 46°, respectively. The 28.56 GHz data were collected during April, May, and June 1978 from the COMSTAR D-2 satellite at an elevation angle of 44°. It is evident from Fig. 1 that effective path length is a strong function of rain rate. In this case the frequency dependence is rather mild; however, in general L_e will depend on frequency; see [5,8]. The frequency dependence arises from the implicit assumption contained in (3) that the rain is uniform at a rate of R_{av} over a path of length L_e. If this were true then effective path length and physical rain extent would be the same, L_e=L, and L_e would not be a function of frequency. The frequency dependence of A and α does not cancel in (3) because the drop size distribution (and thus attenuation) changes with rain rate in a nonlinear fashion. Thus different rain rate distributions with the same average rain rate will lead to different total

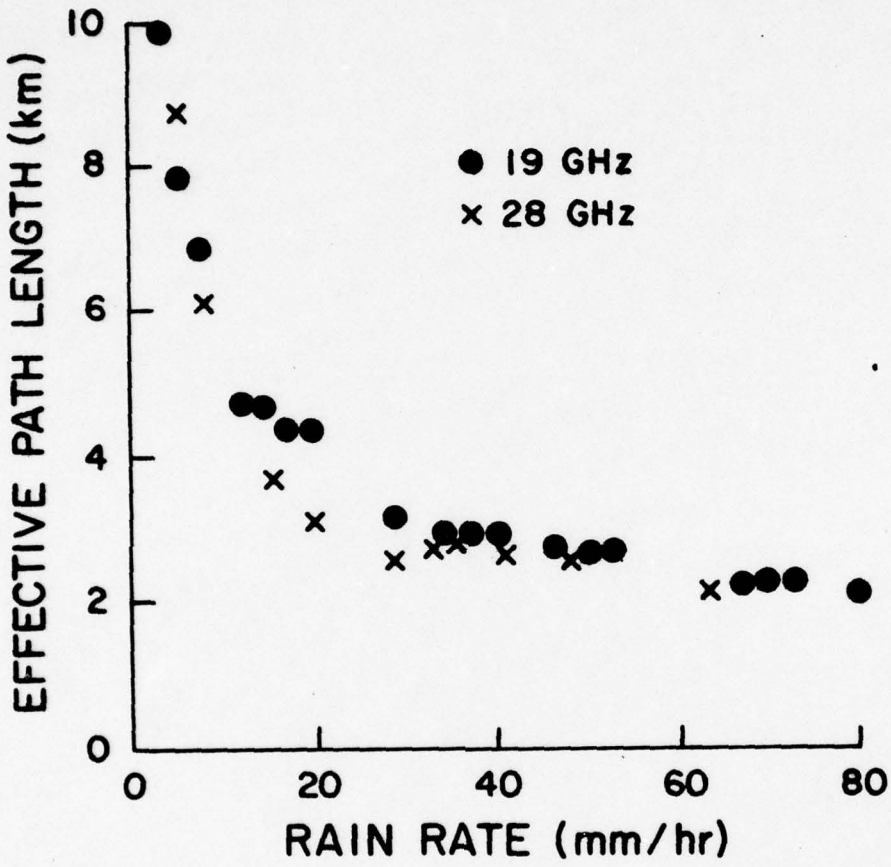

Figure 1. Effective path lengths for the VPI&SU 19.04 and 28.56 GHz COMSTAR experiments (B8 and C10).

attenuations, while specific attenuation remains unchanged because it is based on a uniform rain rate.

For a particular average rain rate (obtained by averaging over a rain gauge network or by a single rain gauge), frequency, and elevation angle, effective path length can be used to predict attenuation from (3) as $A=\alpha L_e$. However, specific attenuation, and thus effective path length, depend upon the wave polarization state and the fraction of oblate drops. Variations of up to 5 dB in the predicted total attenuation can result if the correct system parameters are not used when determining a_1 and b_1.

C. THE SYNTHETIC STORM MODEL

In this section a quasi-physical model of real rains is developed to eliminate the need for effective path lengths. The model accounts for nonuniform rain rates directly and is based on a series of simplifying assumptions which are justified by agreement with experimental results. Based on the data of Fig. 1, two assumptions will be made: 1) rain rate is uniform for low rain rates, and 2) as average rain rate increases, the rain rate distribution $R(\ell)$ becomes increasingly nonuniform.

The first step in the development of the synthetic storm model is the establishment of the effective storm extent. Let the rain be of height H (above a flat earth) and basal length B (in a plane containing the line-of-sight path and local vertical at the earth terminal location). The storm height H follows from the 0°C isotherm height. [9] For simplicity we shall divide the U.S. into site latitude classes giving

$$H = \begin{cases} 3.5 \text{ km} & \text{High-latitude (above 40°)} \\ 4.0 \text{ km} & \text{Mid-latitude} \\ 4.5 \text{ km} & \text{Low-latitude (below 33°)} \end{cases} . \qquad (5)$$

Confidence in these height values can be gained by examining attenuation data from several experiments at different locations, elevation angles, and frequencies. Using attenuation values at 10 mm/hr, where the rain is assumed to be uniform, the rain path length may be determined as $L=A(R=10 \text{ mm/hr})/\alpha$, and α is the calculated specific attenuation at 10 mm/hr for that elevation angle, frequency, polarization, etc. So for each experiment there is a value of L and ε, as indicated in Fig. 2 for a few of the

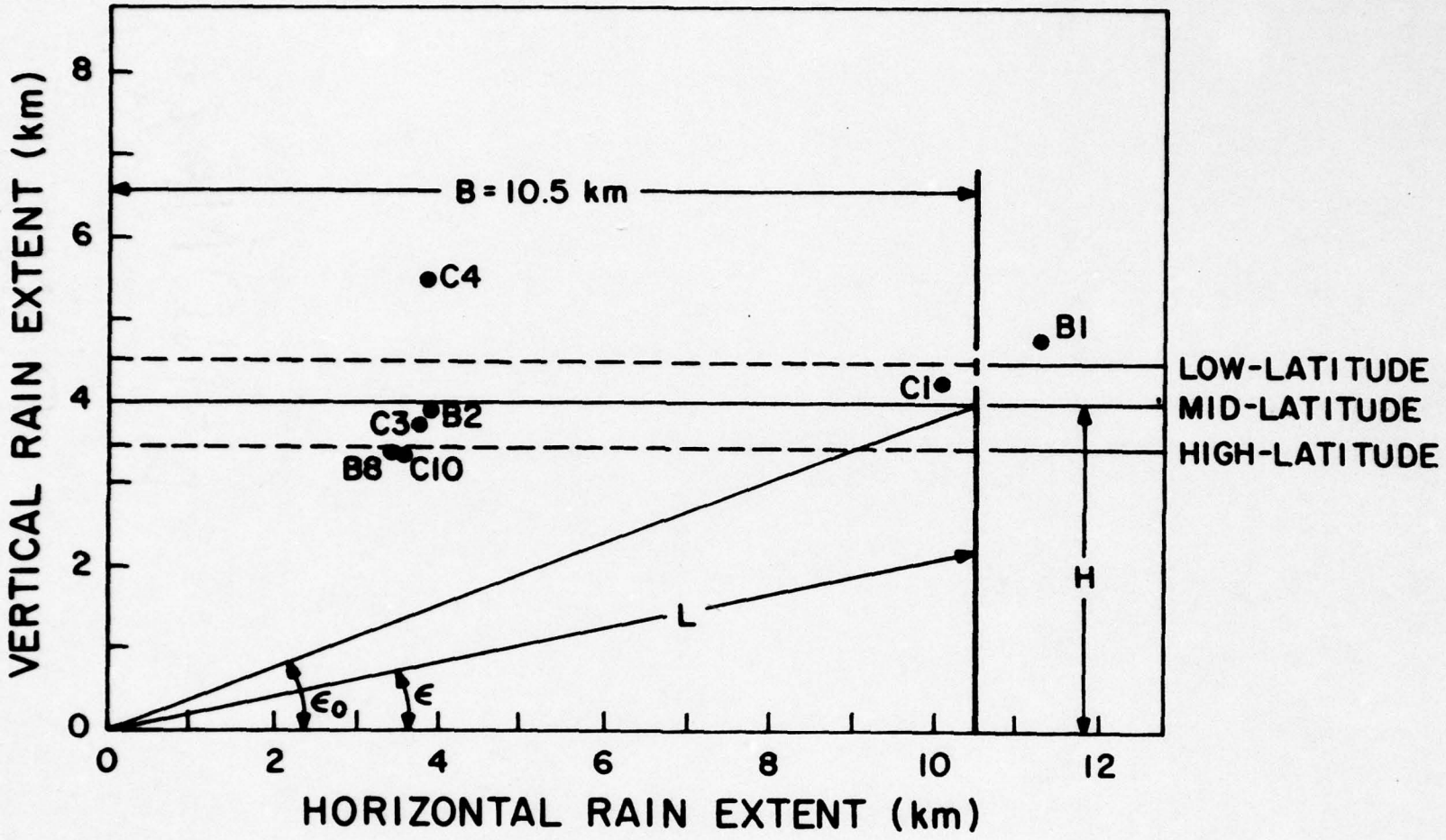

Figure 2. Rain extent model developed from the synthetic storm model.

experiments listed in Table I.* These points also serve as a guide in the selection of the storm basal extent. The value

$$B = 10.5 \text{ km} \tag{6}$$

fits the points C1 and B1 well as shown in Fig. 2. This is a more realistic model than the common assumption of infinite horizontal rain extent. To summarize the storm extent model, the rain path length along a propagation path with elevation angle ε is

$$L = \begin{cases} H \csc \varepsilon & \varepsilon \geq \varepsilon_0 \\ B \sec \varepsilon & \varepsilon \leq \varepsilon_0 \end{cases} \tag{7}$$

where H and B are given in (5) and (6) and ε_0 is $\tan^{-1} \frac{H}{B}$ which is 23.2°, 20.9°, or 18.4° for low, mid, and high latitude classes.

The nonuniform nature of the rain is modeled by dividing the rain path L into N equal intervals, each of which contains rain of uniform rain rate, as shown in Fig. 3. Cell 1 is near the ground antenna of an earth-space link. The rain rates of all cells are related to the rain rate of cell 1, R_1, by the following

$$R_i = \begin{cases} R_1 & R_1 \leq 10 \text{ mm/hr} \\ R_1 \left[\frac{R_1}{10}\right]^{x_i} & R_1 \geq 10 \text{ mm/hr} \end{cases} . \tag{8}$$

where $\{x_i\}$ are real numbers. This relationship includes the uniform

---

* In this report the experiments listed in Table I will be referred to by the code numbers, i.e. A8, C10, etc.

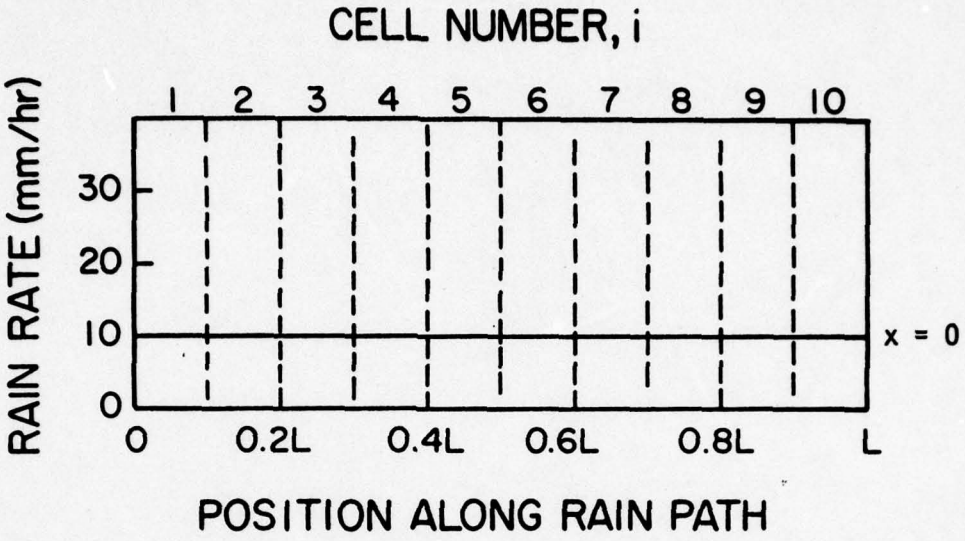

a) Uniform rain of rate 10 mm/hr.

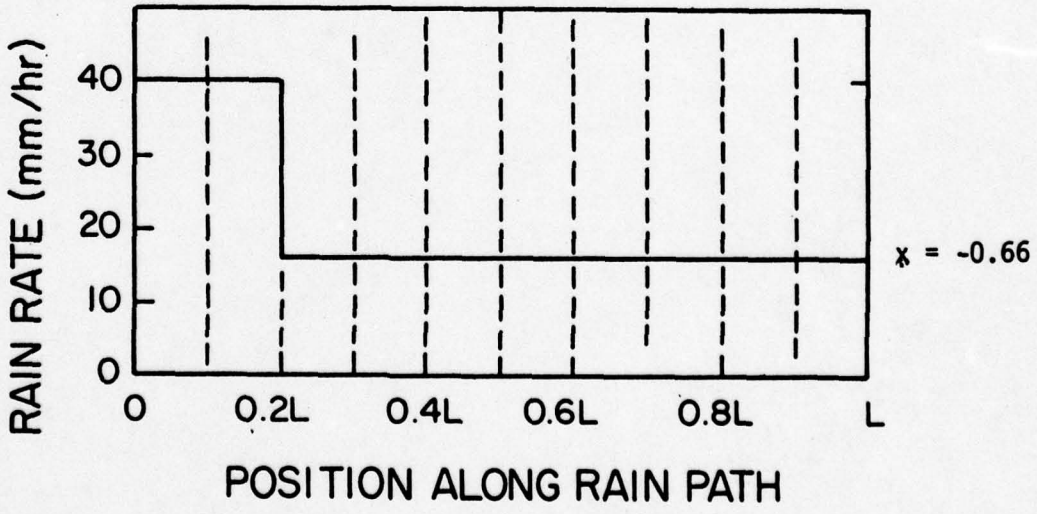

b) Maximum rain rate of 40 mm/hr.

Figure 3. Two level rain rate model for the synthetic storm model; see (10).

rain rate assumption for rates under 10 mm/hr and a piecewise uniform rain model for rates above 10 mm/hr. The total rain attenuation corresponding to this rain rate distribution from (2) is

$$A = \sum_{i=1}^{N} A_i = \frac{L}{N} \sum_{i=1}^{N} \alpha(R_i) \qquad \text{dB} \tag{9}$$

where A_i and R_i are the total attenuation and rain rate for the i^{th} cell.

The general model of (8) and (9) has unknowns N and $\{x_i\}$. To simplify the solution a ten-cell, two-level rain rate model was selected. The unknowns are then C, the fraction of the path over which the rain rate R_1 extends and which is a multiple of 0.1L, and x, the parameter which specifies the rain rate of the remaining cells, i.e.

$$R_x = \begin{cases} R_1 & R_1 \leq 10 \text{ mm/hr} \\ R_1 \left[\frac{R_1}{10}\right]^x & R_1 \geq 10 \text{ mm/hr} \end{cases} . \tag{10}$$

The attenuation expression (9) then reduces to

$$A = [C\,\alpha(R_1) + (1-C)\,\alpha(R_x)]L \qquad \text{dB} \quad . \tag{11}$$

Attenuation and rain rate data pairs for the experiments B1, B8, C1, C4, and C10 listed in Table I were used to determine x and C such that the predicted attenuation from (10) and (11) best fit the measured values over the range of rain rates for the experiments. Specific attenuation parameters a_1 and b_1 in (1) were computed for the elevation angle, frequency, polarization, etc. of the experiment. [5] The best fit results

are

$$x = -0.66 \quad \text{and} \quad C = 0.2 \; . \tag{12}$$

This result was also obtained earlier [5,16,17] by examining attenuation data for a single experiment (VPI&SU COMSTAR 28.56 GHz summer 1977 data) and a single rain rate (R_1=40 mm/hr). We also note that a two-level rain rate distribution for terrestrial paths has yielded good agreement to attenuation measurements. [18]

Theoretical predictions using (10) - (12) and the values of L in Table I are compared to measured data in Fig. 4 for 20 and 30 GHz and in Fig. 5 for 11 GHz. Specific attenuation parameters a_1 and b_1 used in (11) were developed using the Rain Propagation Prediction model of [5] for the polarization state, frequency, and elevation angle of the experiment. Also, a mixture of 40% spherical and 60% oblate rain drops with a zero mean, 12° standard deviation normal distribution of canting angles was used to generate a_1 and b_1. Note that in Fig. 4 agreement is very good for various locations, frequencies, elevation angles, etc. Predictions for 11.7 GHz are, however, consistently low as noted by the data from three experiments shown in Fig. 5. This discrepancy is possibly due to storms which pass through the propagation path but not over the site rain gauge. This effect is one of a lower than actual rain rate for a given attenuation and is more pronounced at 11 GHz than at 20 or 30 GHz because of the higher rain rates required for noticeable attenuation at 11 GHz. In any event, the model may be verified at 11 GHz by examining isolation versus attenuation, which removes the point rainfall rate dependence. Experimental data and theoretical predictions [5] based on the two-level rain distri-

Table 1

Characteristics of Several Millimeter Wave Satellite Propagation Experiments

Code	Frequency (GHz)	Elevation Angle	Rain Path Length L(km)	Site	Site Latitude	Data Period	Satellite
A8	11.7	49°	5.963	U. of Texas Austin, TX [10]	30°	Oct. 18, 1976- Jan. 31, 1978	CTS
A9	11.7	24°	8.605	GTE Labs Waltham, MA [11]	42°	June 1977- Jan. 1978	CTS
A13	11.7	33°	7.344	VPI&SU Blacksburg, VA [3]	37°	1978	CTS
A15	11.7	27°	8.811	Bell Labs Crawford Hill, NJ [12]	40°	April 26, 1976- April 26, 1977	CTS
B1	19.04	23°	10.237	Comsat Labs Clarksburg, MD [13]	39°	July 1976- January 1977	COMSTAR D-1
B2	20.0	45°	5.657	NASA Rosman, NC [15]	35°	July-Dec. 1974	ATS-6
B8	19.04	45°	5.657	VPI&SU Blacksburg, VA [3]	37°	1978	COMSTAR D-2/D-3
C1	28.56	23°	10.237	Comsat Labs Clarksburg, MD [13]	39°	July 1976- January 1977	COMSTAR D-1
C3	30.0	45°	5.657	NASA Rosman, NC [15]	35°	July-Dec. 1974	ATS-6
C4	30.0	55°	5.493	U. of Texas Austin, TX [14]	30°	July 1974- May 1975	ATS-6
C10	28.56	44°	5.758	VPI&SU Blacksburg, VA [3]	37°	April, May, June 1978	COMSTAR D-2

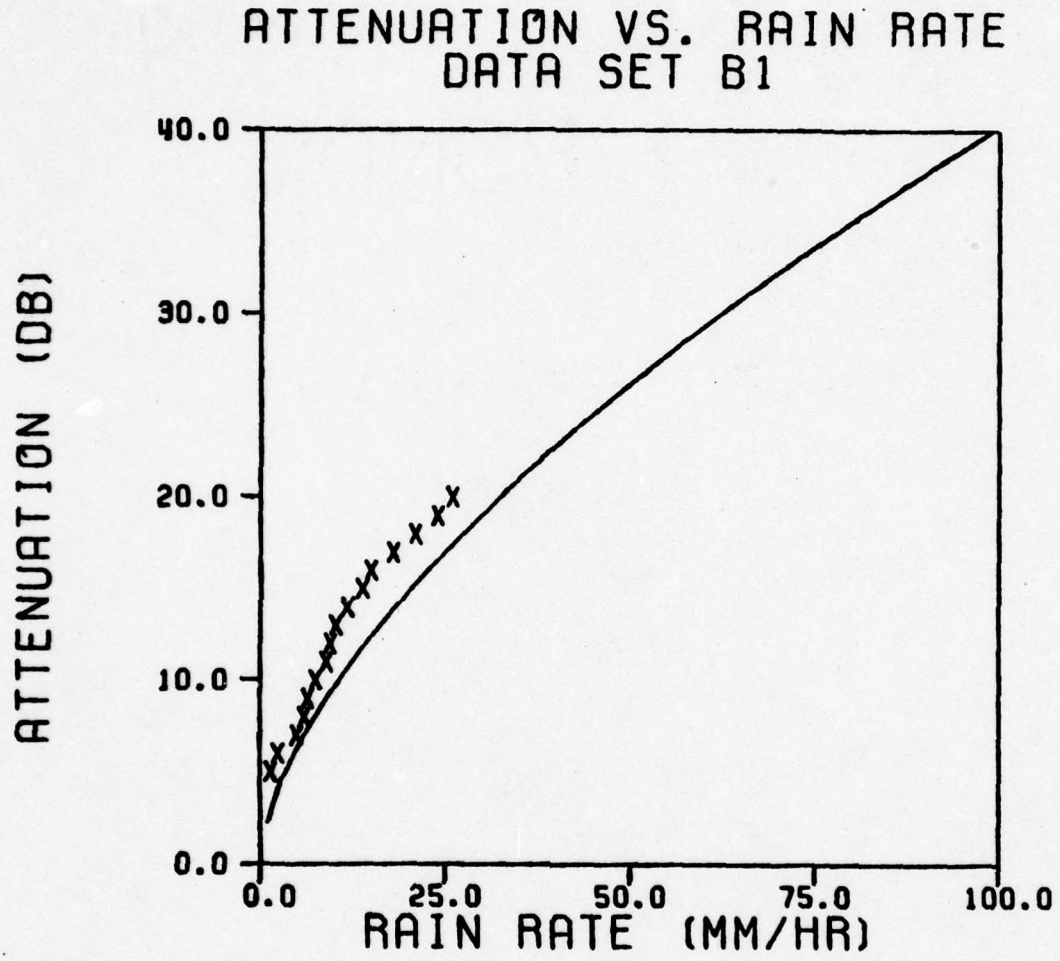

Figure 4a. Measured data from the Comsat Labs. COMSTAR D-1 19.04 GHz experiment (B1) compared to predicted results from the synthetic storm model (solid curve).

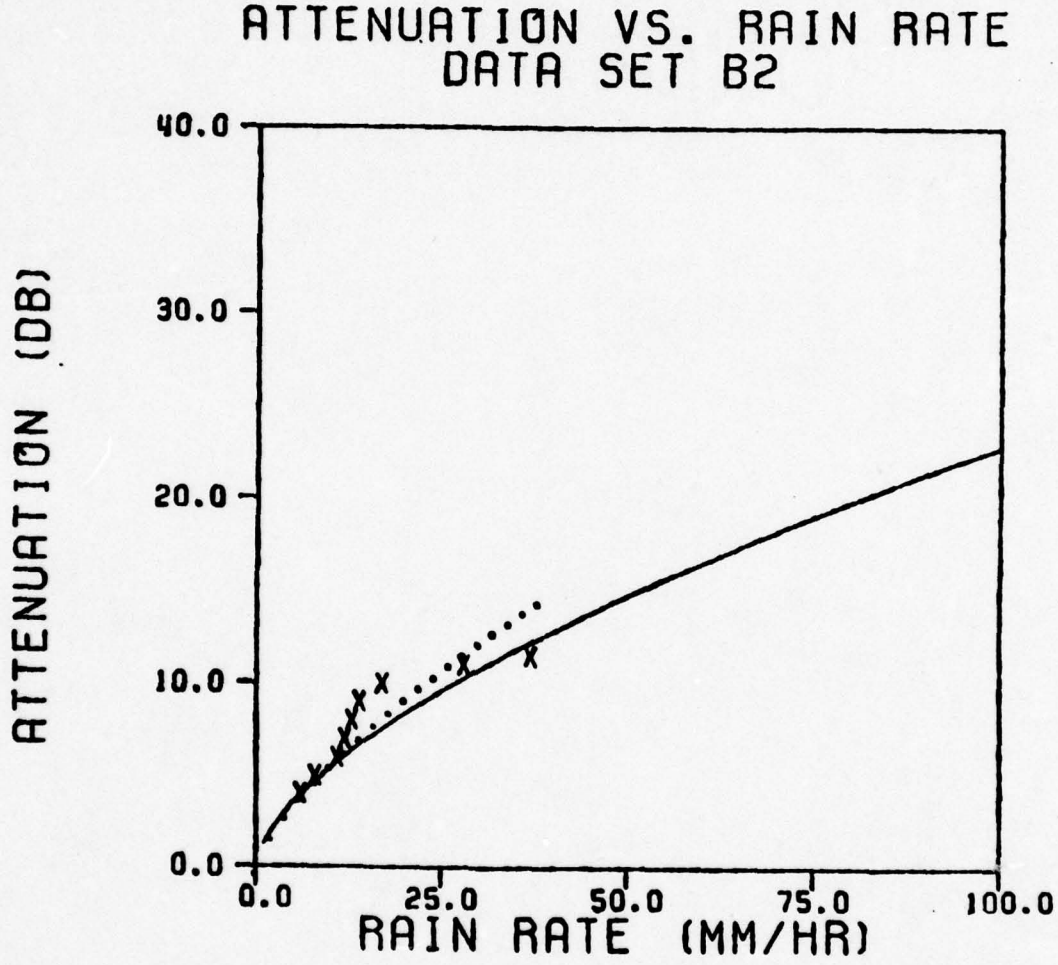

Figure 4b. Measured data from the NASA Rosman ATS-6 20 GHz experiment (B2) compared to predicted results from the synthetic storm model (solid curve). The dotted curve is a fit to the data given by $1.1547\ R^{0.6998}$.

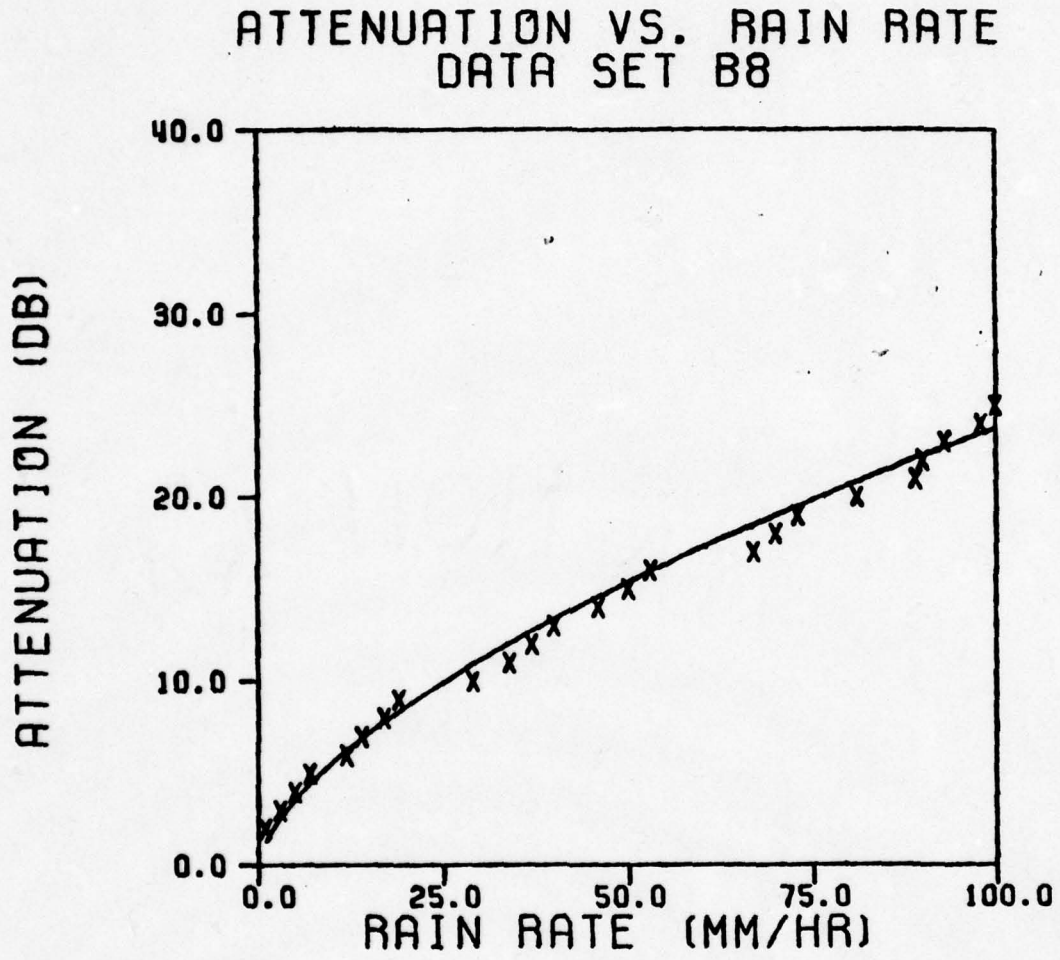

Figure 4c. Measured data from the VPI&SU COMSTAR D-2/D-3 19.04 GHz experiment (B8) compared to the predicted results from the synthetic storm model (solid curve).

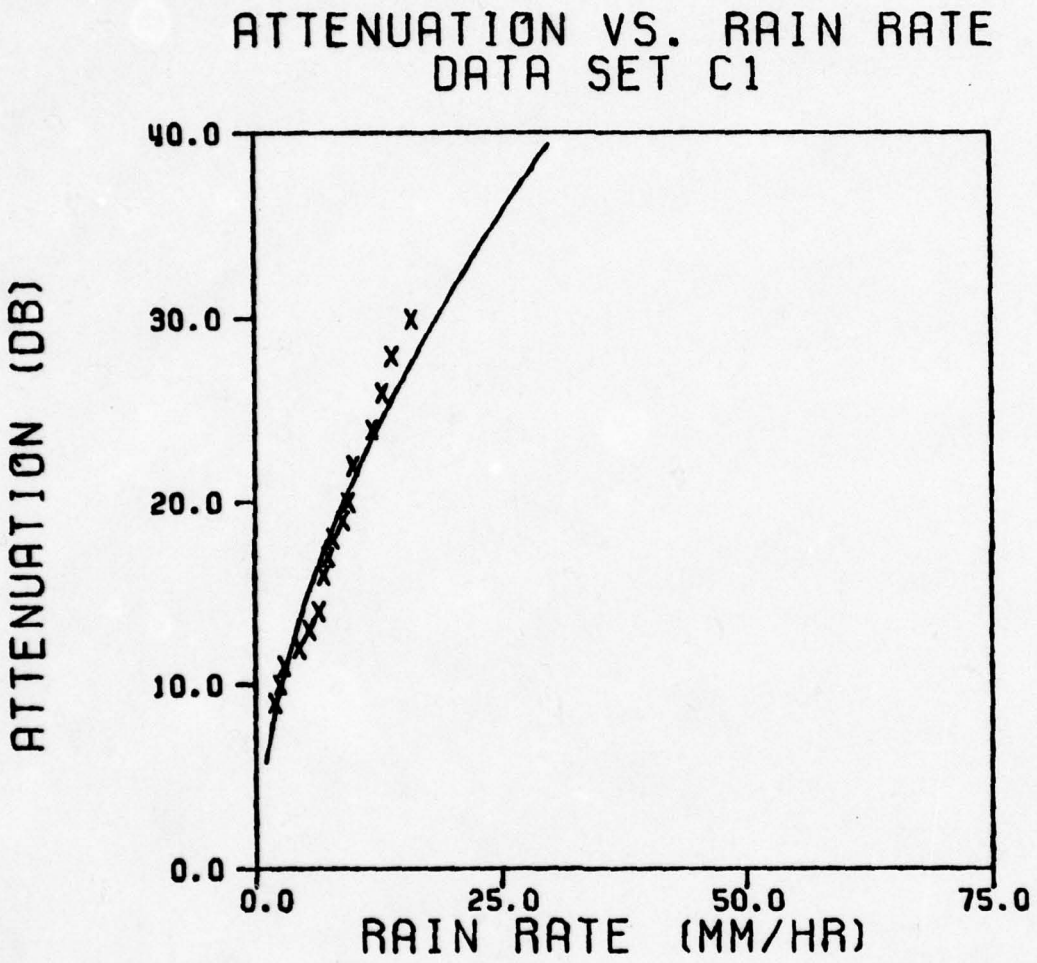

Figure 4d. Measured data from the Comsat Labs. COMSTAR D-1 28.56 GHz experiment (C1) compared to predicted results from the synthetic storm model (solid curve).

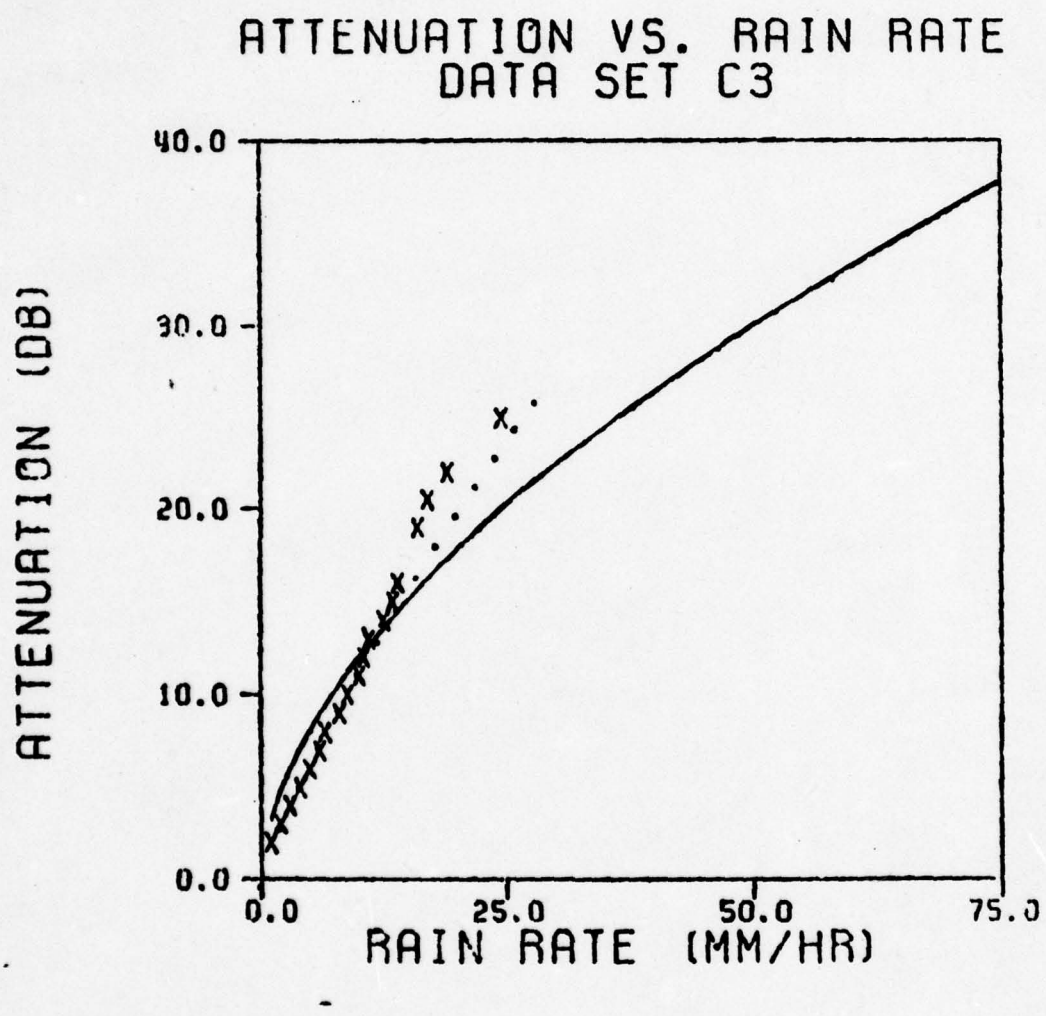

Figure 4e. Measured data from the NASA Rosman ATS-6 30 GHz experiment (C3) compared to predicted results from the synthetic storm model (solid curve). The dotted curve is a fit to the data given by $1.7748\ R^{0.8081}$.

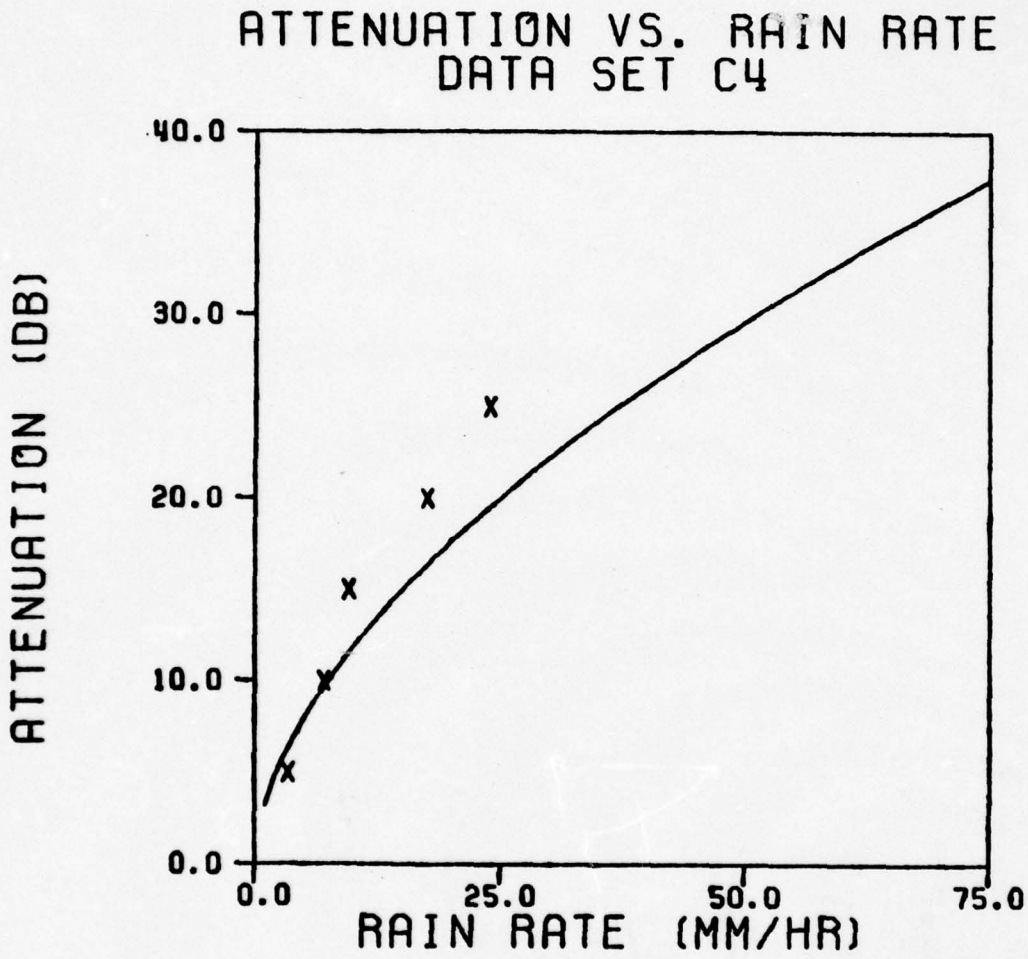

Figure 4f. Measured data from the U. of Texas ATS-6 30 GHz experiment (C4) compared to predicted results from the synthetic storm model (solid curve).

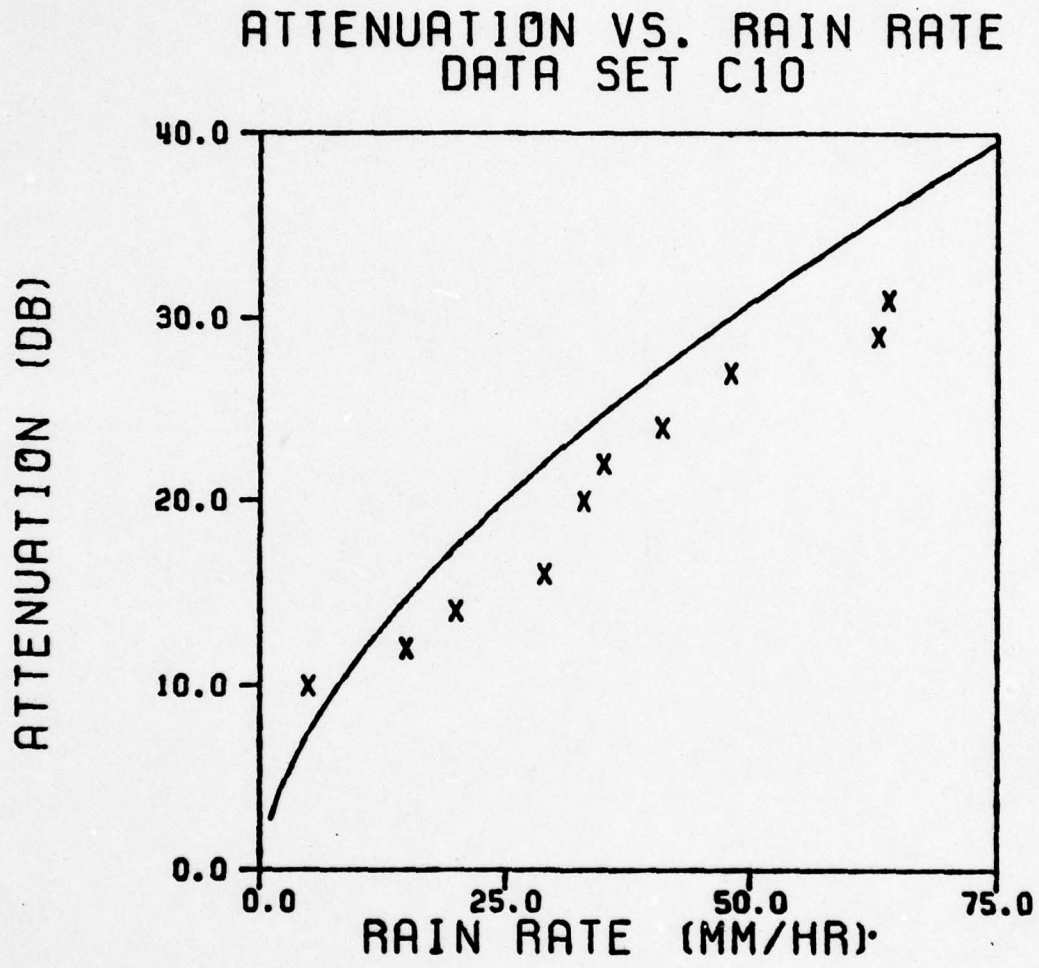

Figure 4g. Measured data from the VPI&SU COMSTAR D-2 28.56 GHz experiment (C10) compared to predicted results from the synthetic storm model (solid curve).

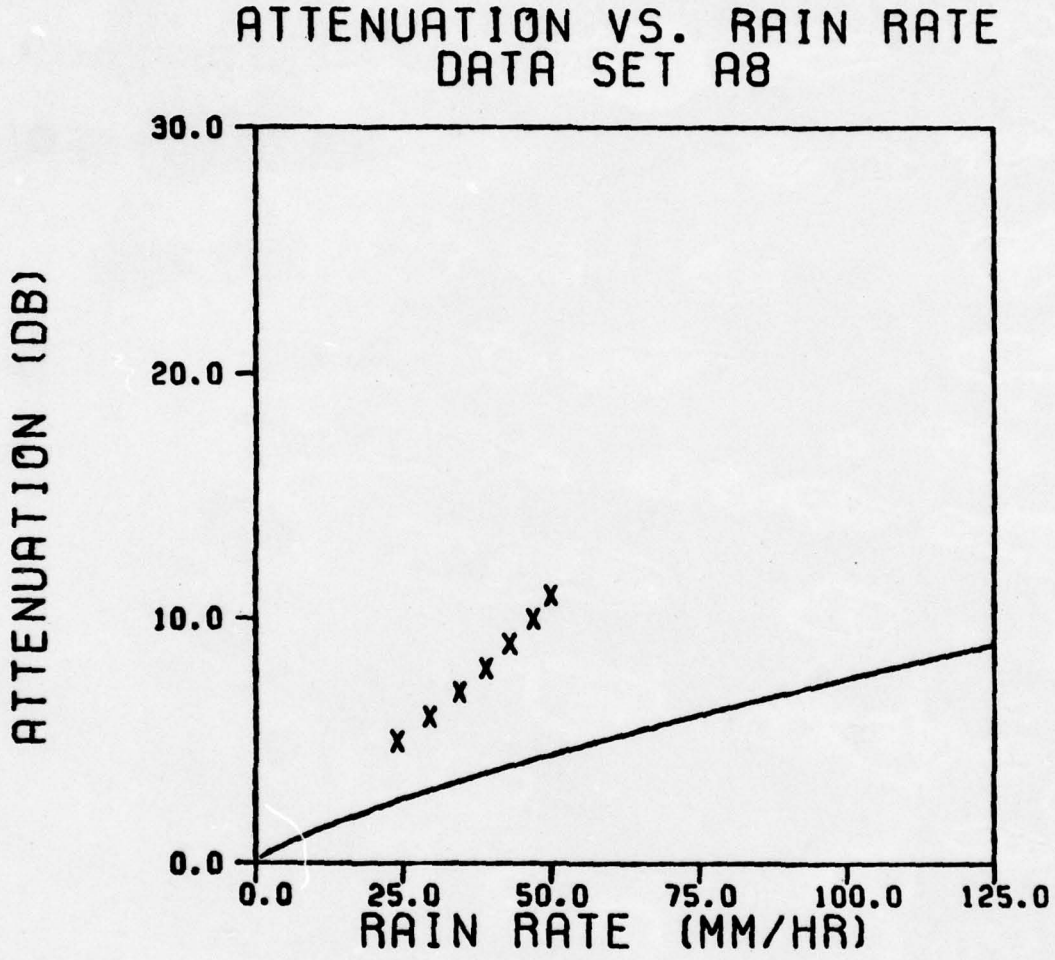

Figure 5a. Measured data from the U. of Texas CTS 11.7 GHz experiment (A8) compared to predicted results from the synthetic storm model (solid curve).

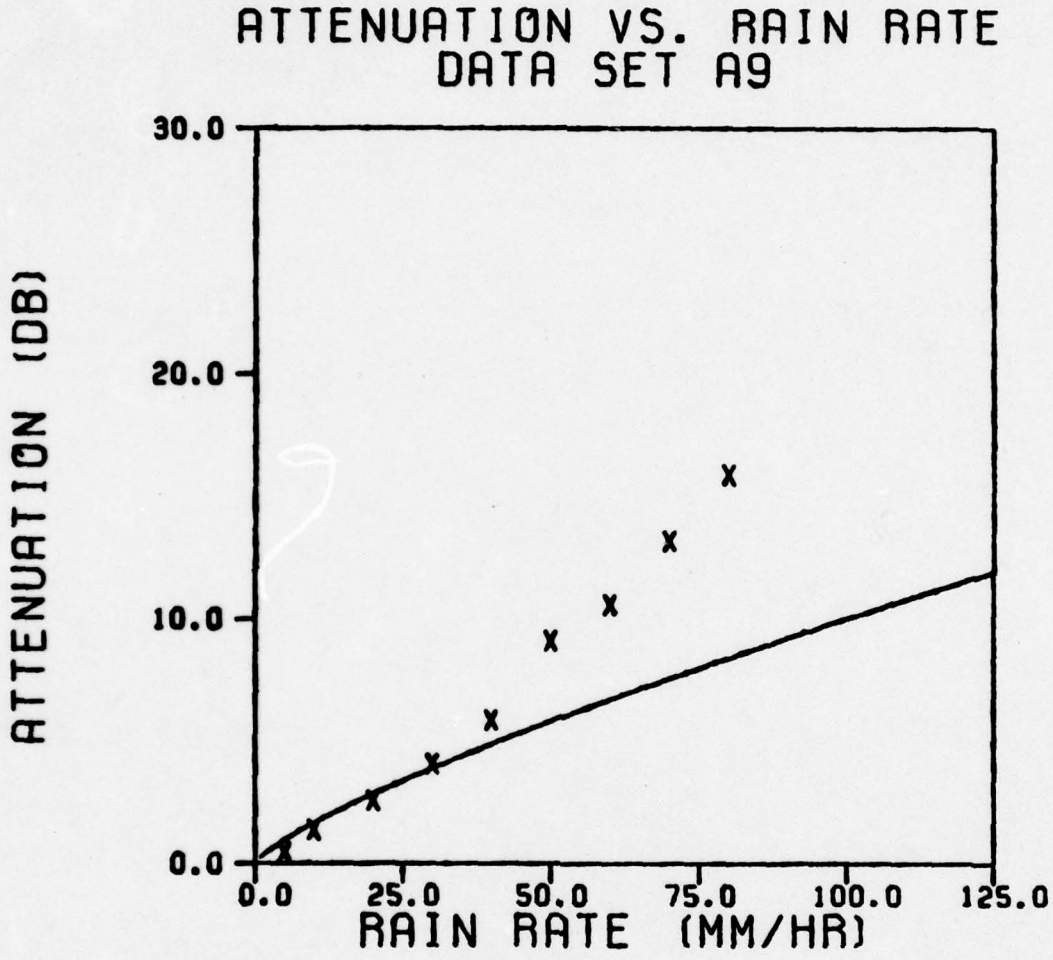

Figure 5b. Measured data from the GTE Labs. CTS 11.7 GHz experiment (A9) compared to the predicted results from the synthetic storm model (solid curve).

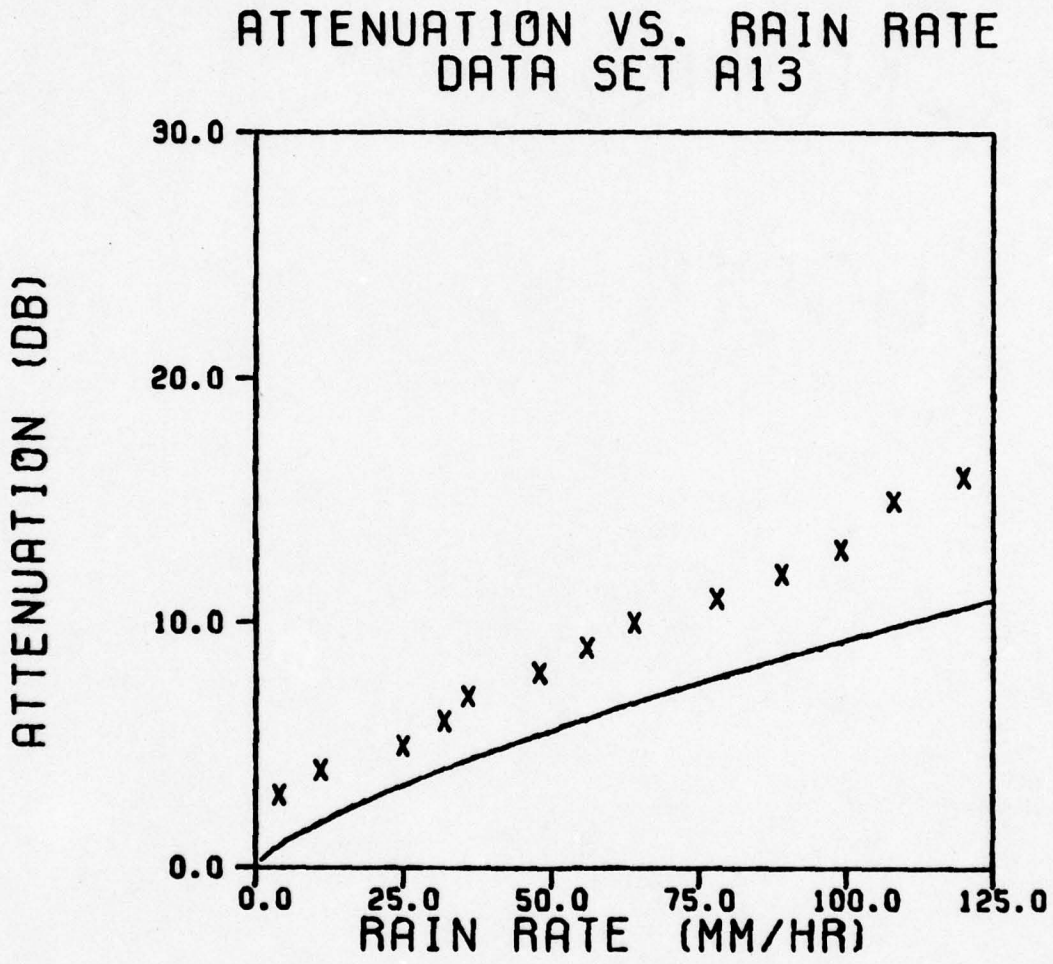

Figure 5c. Measured data from the VPI&SU CTS 11.7 GHz experiment (A13) compared to predicted results from the synthetic storm model (solid curve).

bution model are shown in Fig. 6. Note the good agreement for all three experiments.

Recently Hodge [19] has proposed a method for frequency scaling of attenuation. Assuming a Gaussian spatial distribution of rain rate the ratio of attenuations A" and A' at frequencies f" and f' is

$$\frac{A''}{A'} = \frac{a_1''}{a_1'} R^{b_1'' - b_1'} \sqrt{\frac{b_1'}{b_1''}} \tag{13}$$

where R is the maximum of the rain rate distribution and a_1', b_1', a_1'', and b_1'' are the power law fit coefficients for specific attenuations as in (1). Using the specific attenuations for 30 GHz and 20 GHz at an elevation angle of 44° in (13) gives

$$\frac{A(30)}{A(20)} = 2.49\ R^{-0.0528}\ . \tag{14}$$

The synthetic storm model results yield

$$\frac{A(30)}{A(20)} = 2.57\ R^{-0.0612}\ . \tag{15}$$

This and the Hodge model of (14) are plotted in Fig. 7. Note the excellent agreement between the two the etical predictions. Attenuation ratio data is plotted in Fig. 8 for the 28.56 and 19.04 GHz data from the VPI&SU COMSTAR D-2 experiment during April to June, 1978, as a function of 19 GHz attenuation. The bars indicate the standard deviation of the data. The solid curve is the theoretical prediction using the synthetic storm model. These attenuation ratio results (both theory and data) are in good agreement with that reported for ATS-6 30 and 20 GHz measurements [14,20,21], as well as for other COMSTAR 28 and 19 GHz measurements [13].

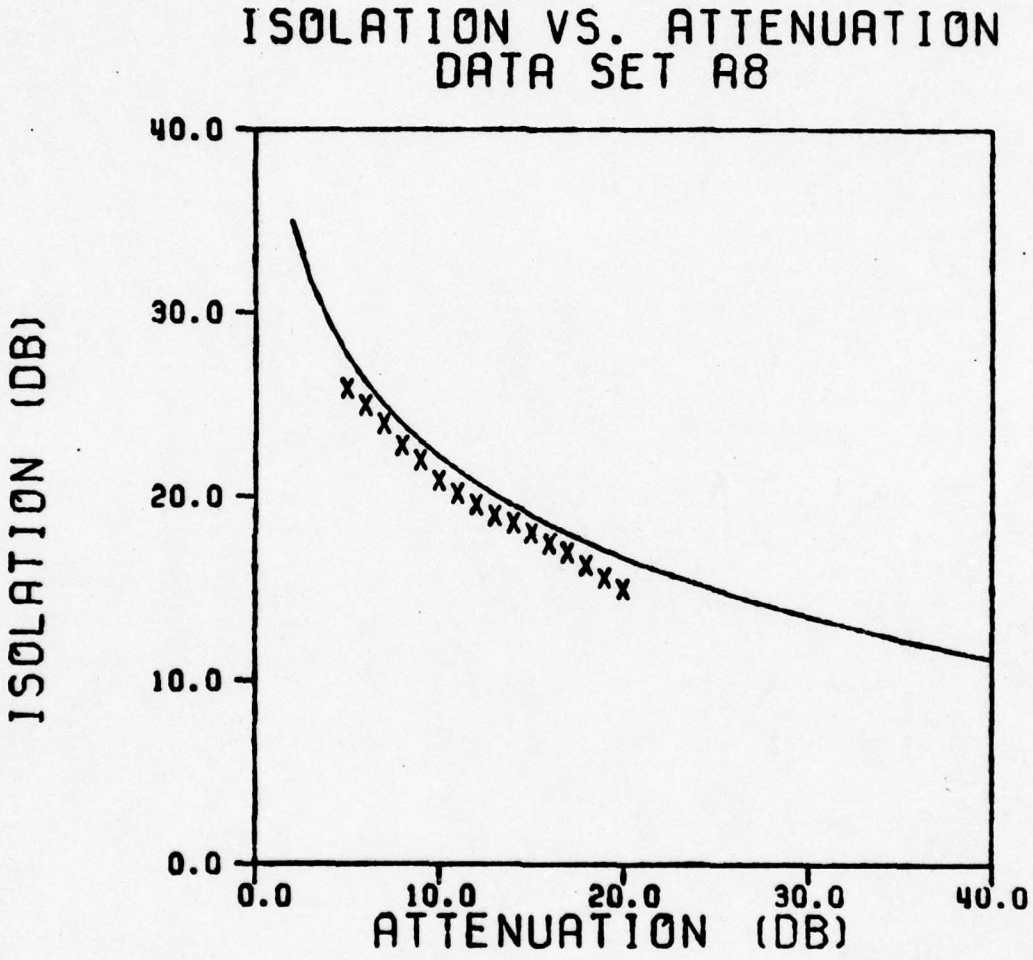

Figure 6a. Isolation versus attenuation data from the U. of Texas CTS 11.7 GHz experiment (A8) compared to predicted results from the synthetic storm model (solid curve).

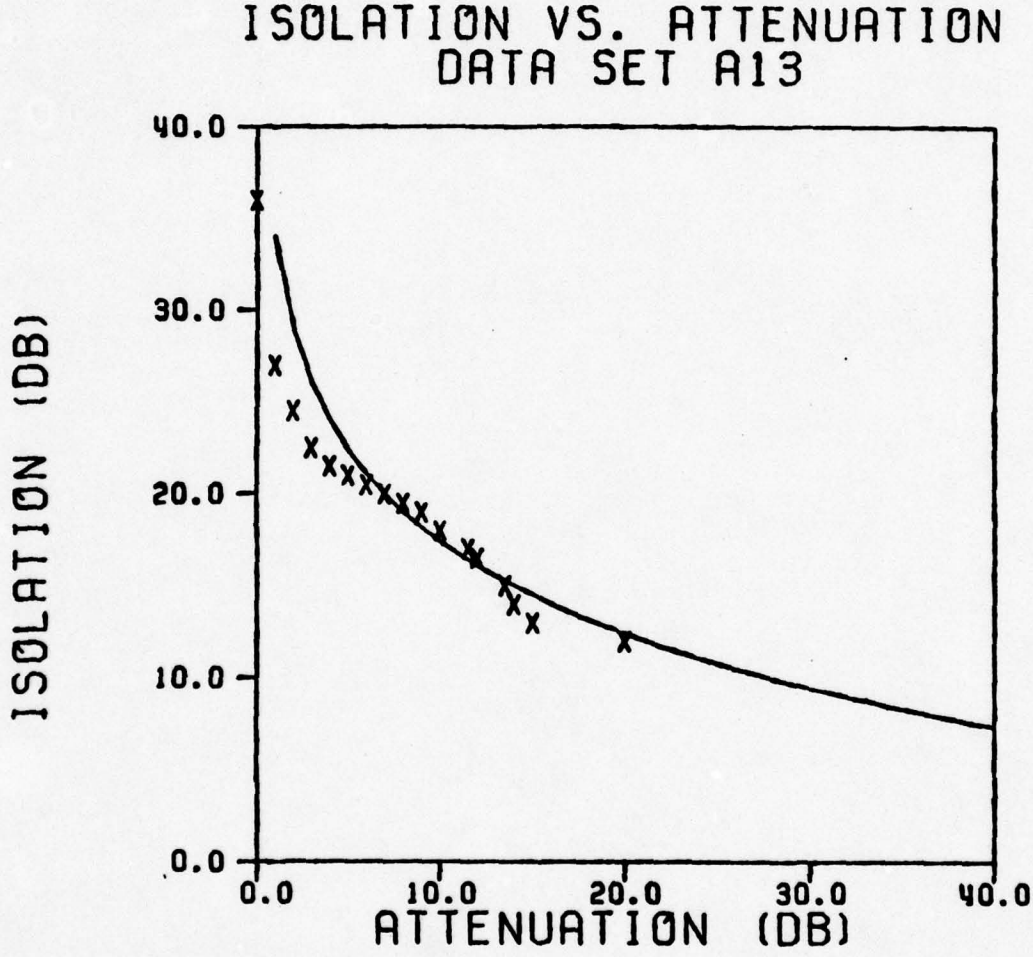

Figure 6b. Isolation versus attenuation data from the VPI&SU CTS 11.7 GHz experiment compared to predicted results from the synthetic storm model (solid curve).

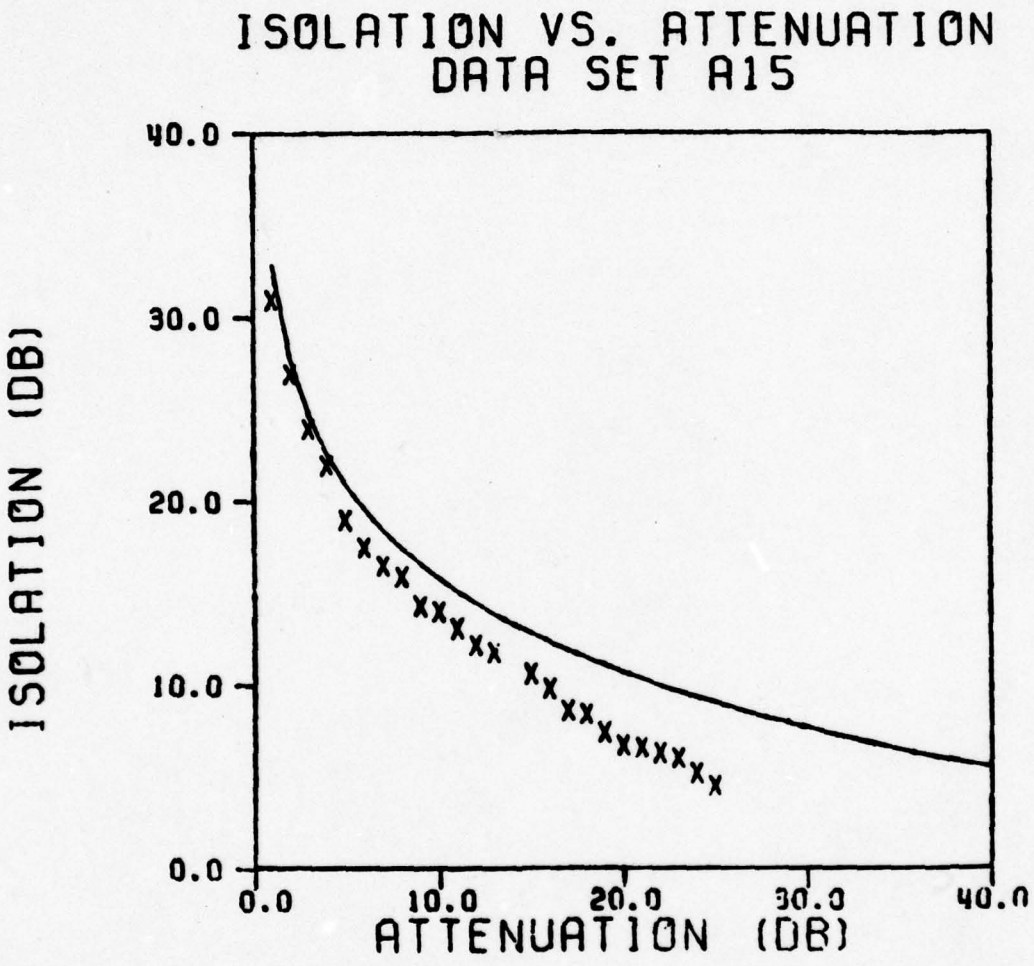

Figure 6c. Isolation versus attenuation data from the Bell Labs. CTS 11.7 GHz experiment (A15) compared to predicted results from the synthetic storm model (solid curve).

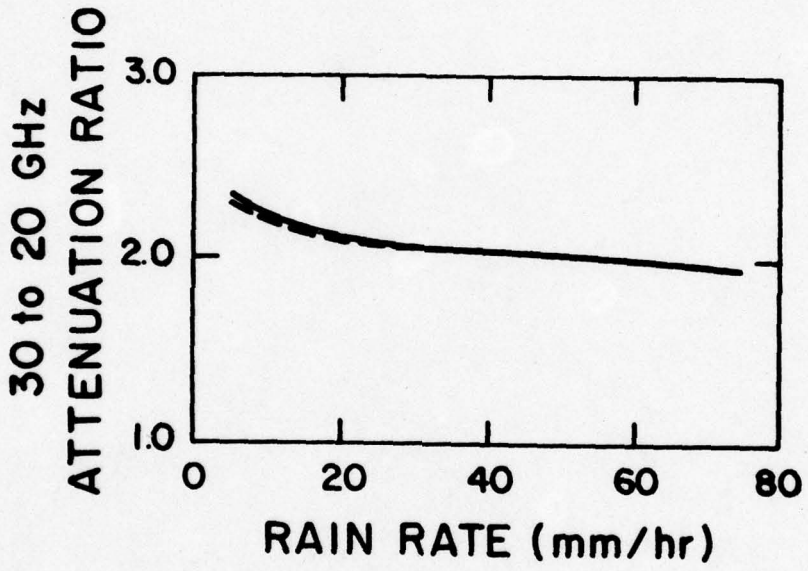

Figure 7. Ratio of rain attenuation at 30 GHz to that at 20 GHz as a function of rain rate computed from the synthetic storm model (solid curve) and from the Hodge model (dashed curve). The elevation angle is 44°.

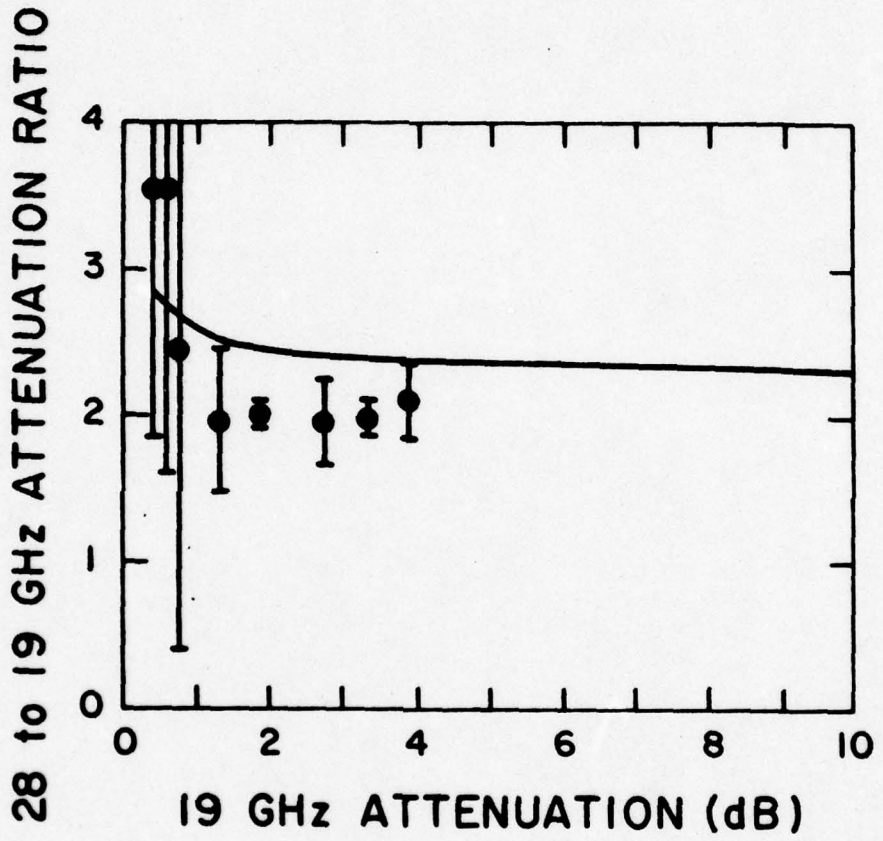

Figure 8. Ratio of 28.56 GHz attenuation to that at 19.04 GHz measured at VPI&SU from the COMSTAR D-2 satellite during April, May, and June of 1978. Error bars indicate one standard deviation. The solid curve is that predicted using the synthetic storm model.

D. ATTENUATION PREDICTION USING RAINFALL ACCUMULATION

The least expensive method for predicting rain attenuation statistics on an earth-space link would involve the use of ground rainfall accumulation data only. This approach is very desirable for evaluating earth station locations, because widely available rainfall accumulation data used to predict attenuation statistics would provide system outage estimates. The general solution to this problem is in its infancy, but in this section the synthetic storm model will provide some encouraging results.

The Rice-Holmberg rain rate model [6] provides a method of predicting rain rate statistics from rain accumulation data. It yields the percent of time that rain rate R is exceeded over a time period P in hours during which M millimeters of rain fell as follows

$$\%T(R) = R_0\{[0.03\ \beta\ e^{-0.03R} + 0.2(1 - \beta)[e^{-0.258R} + 1.86\ e^{-1.63R}]\} \qquad (16)$$

where $R_0 = 100\ M/P$ and β is the ratio of accumulation of "thunder storm rain" to the total rain accumulation. The attenuation results from the synthetic storm model can be fitted to a power curve giving $A = aR^b$ which in turn can be solved for R as

$$R = \exp[b^{-1}\ \ln(\frac{A}{a})]\ . \qquad \text{mm/hr} \qquad (17)$$

Using (17) in (16) will yield the percent of time that attenuation A is exceeded.

This procedure was tested with statistical rain and attenuation data collected at the VPI&SU earth station for the calendar year 1978. During that time (P = 8766 hr) a total rain accumulation of M=434 mm was

measured. The fraction of thunderstorm rain β was chosen to be 0.2 from the ratio of rain accumulation for rates above 30 mm/hr to the total accumulation; this value agrees with that in [6]. These values in (16) yield the solid curve in Fig. 9. Also shown are the measured rain rate statistical data. Note the excellent agreement to the simple Rice-Holmberg model.

The theoretical predictions of attenuation statistics using the predicted rain rate statistics of Fig. 9 and the attenuation relationships from the synthetic storm model are plotted as the solid curves in Fig. 10. The measured data for the COMSTAR (28.56 and 19.04 GHz) and CTS (11.7 GHz) experiments are also shown. Agreement is very good, except for a slight shift between theory and experiment for CTS which was noted previously for several CTS experiments.

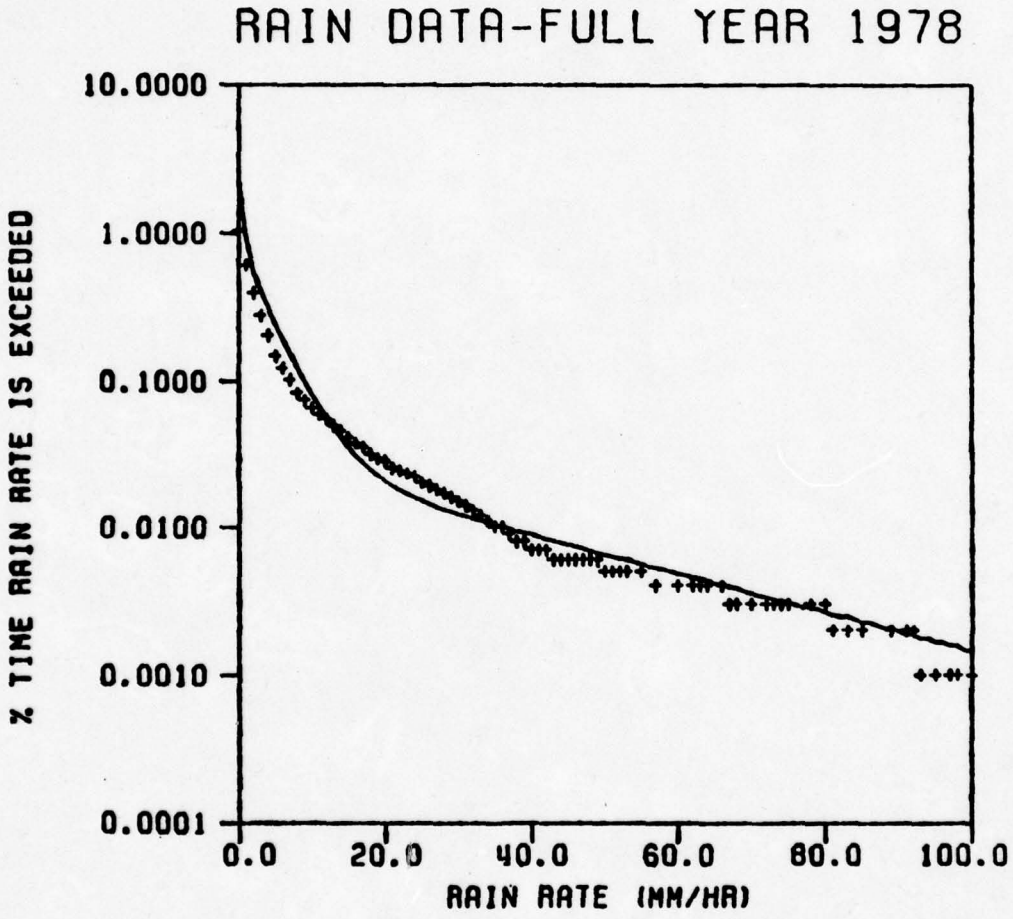

Figure 9. Rain rate exceedence for the year of 1978 as measured at VPI&SU. The solid curve is that predicted by the Rice-Holmberg model (β=0.2).

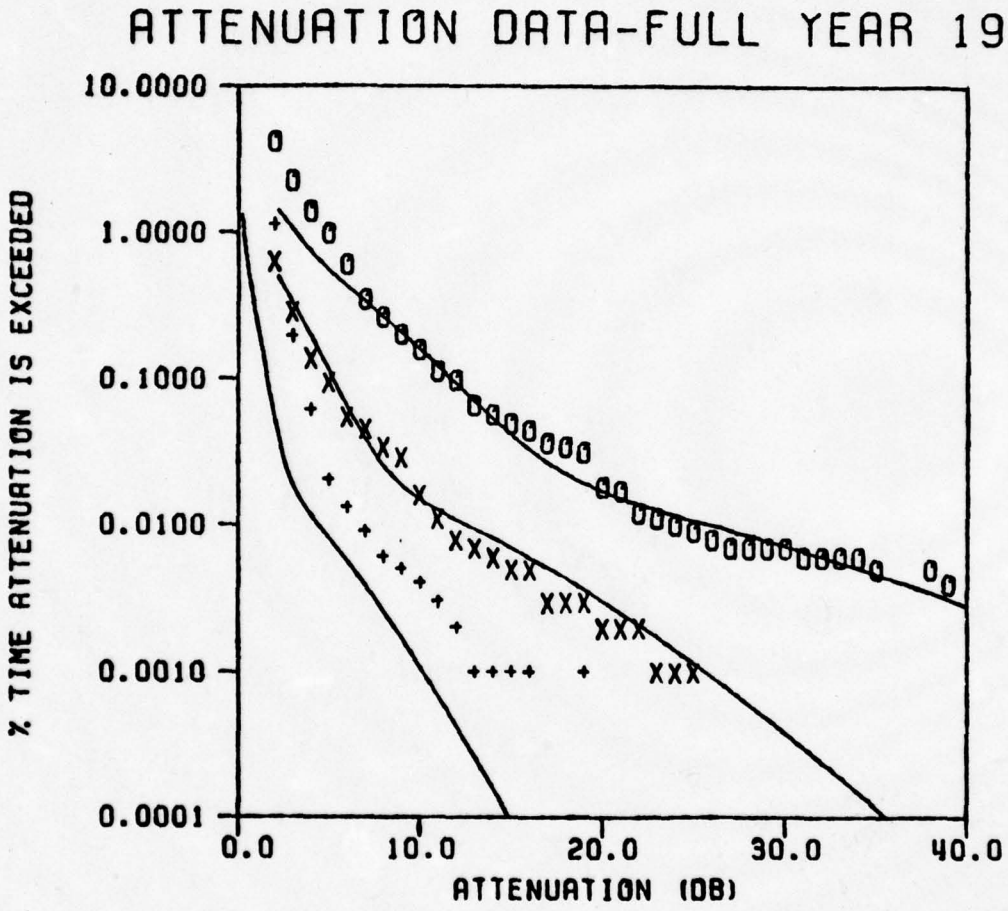

Figure 10. Attenuation exceedence for the year of 1978 measured at VPI&SU at three frequencies: 28.56 GHz (O), 19.04 GHz (X), and 11.7 GHz (+). The solid curves are those predicted from the Rice-Holmberg rain rate of Fig. 9 and the attenuation-rain rate relationships from the synthetic storm model.

E. CONCLUSIONS

This part of the report has illustrated that the effective path length model for predicting total attenuation from specific attenuation has limited application. The synthetic storm model was proposed as an alternative. The piecewise uniform rain rate model with N cells along the rain portion of the communication path appears to have sufficient flexibility for a variety of modeling applications. Good agreement to experimental results was obtained using only two rain rate levels along the path. As a larger data base for many frequencies, locations, and elevation angles becomes available, a larger portion of the model flexibility may yield further improvements, as well as permitting models for particular climatic zones. Experimental confirmation demonstrated the tendency of the model to be independent of frequency, location, and elevation angle.

It was also shown that the synthetic storm model can be used to scale attenuation from one frequency to another. In addition, together with the Rice-Holmberg rain rate model the synthetic storm model can be used to predict attenuation statistics from ground rainfall accumulation alone.

F. REFERENCES

1. C. W. Bostian, et. al., "Final Report (Second Year of Work) on a Depolarization and Attenuation Experiment Using the COMSTAR and CTS Satellites," NASA Goddard Contract NAS5-22577, Feb. 9, 1978.

2. C. W. Bostian, et. al., "A Depolarization and Attenuation Experiment Using the COMSTAR and CTS Satellites - Data Report for December 1976 through March 1978," NASA Goddard Contract NAS5-22577, April 28, 1978.

3. C. W. Bostian, et. al., "A Depolarization and Attenuation Experiment Using the COMSTAR and CTS Satellites - Final Report for the Third Year of Work," NASA Goddard Contract NAS5-22577, Feb. 9, 1979.

4. C. W. Bostian, et. al., "Quarterly Technical Progress Report I on a Depolarization and Attenuation Experiment Using the COMSTAR and CTS Satellites," NASA Goddard Contract NAS5-22577, Dec. 22, 1976.

5. R. R. Persinger and W. L. Stutzman, "A Depolarization and Attenuation Experiment Using the CTS and COMSTAR Satellites - Millimeter Wave Propagation Modeling of Inhomogeneous Rain Media for Satellite Communication Systems," Interim Report 1978-1, NASA Goddard/DCA Contract NAS5-22577 and U.S. Army Research Office Grant DAAG29-77-G-0083, June, 1978.

6. P. L. Rice and N. R. Holmberg, "Cumulative time statistics of surface-point rainfall rates," *IEEE Trans. on Comm.*, vol. COM-21, pp. 1131-36, Oct. 1973.

7. R. L. Olsen, D. V. Rogers, and D. B. Hodge, "The a R^b relation in the calculation of rain attenuation, *IEEE Trans. Antennas Propagat.*, vol. AP-26, pp. 318-329, March 1978.

8. L. J. Ippolito, "Attenuation statistics at 11.7 GHz - long term measurement and prediction techniques," 1978 URSI/USNC Spring Meeting, College Park, Maryland, May 15-19, 1978.

9. R. Kaul, "Prediction of Attenuation on Earth-Space Paths," in "Prediction of Millimeter Wave Propagation Effects on Earth-Space Paths," Technical Report 1418, NASA/Goddard, Dec. 1978.

10. W. J. Vogel and A. W. Straiton, "CTS Attenuation and Crosspolarization Measurements at 11.7 GHz," Final Report under NASA Contract NAS5-22576, Sept. 1978.

11. O. G. Nackoney, "CTS 11.7 GHz Propagation Measurements: First Year's Data Report," GTE Labs. Technical Note TR78-471.1, Sept. 1978.

12. A. J. Rustako, "An Earth-Space Propagation Measurement at Crawford Hill Using the 12-GHz CTS Satellite Beacon," *BSTJ*, vol. 57, pp. 1431-1448, May-June 1978.

13. J. M. Harris and G. Hyde, "Preliminary results of COMSTAR 19/29 GHz beacon measurements at Clarksburg, Maryland," *Comsat Technical Review*, vol. 7, pp. 599-623, Fall 1977.

14. L. J. Ippolito, "20- and 30-GHz millimeter wave experiments with the ATS-6 satellites," NASA TND-8197, p. 2-24, April 1976.

15. L. J. Ippolito, "Rain Attenuation Prediction at 10 to 100 GHz from Satellite Beacon Experiments," EASCON '78, Arlington, VA, Sept. 1978.

16. R. R. Persinger and W. L. Stutzman, "A rain propagation prediction model for earth-space millimeter wave signals," URSI/USNC Spring Meeting, College Park, Maryland, May 1978.

17. R. E. Castle and C. W. Bostian, "Propagation modeling for system design," URSI/USNC Spring Meeting, College Park, Maryland, May 1978.

18. M. S. Assis and C. M. Einloft, "A simple method for estimating rain attenuation distribution," *Proceedings of the URSI Commission F Open Symposium*, LaBaule, France, May 1977.

19. D. B. Hodge, "Frequency scaling of rain attenuation," *IEEE Trans. Antennas and Propagat.*, vol. AP-25, pp. 446-447, May 1977.

20. R. G. Howell and J. Thirwell, "20 GHz Cross-Polarization and Dual Frequency Attenuation and Scintillation Measurements Using the ATS-6 Satellite," URSI Commission F Open Symposium (LaBaule, France) Proceedings, pp. 339-344, May 1977.

21. D. J. Fang and J. M. Harris, "Precipitation Attenuation Studies Based on Measurements of ATS-6 20/30 GHz Beacon Signals at Clarksburg, MD," *IEEE Trans. on Ant. and Prop.*, vol. AP-27, pp. 1-11, Jan. 1979.

PART II

RECIPROCITY AND MILLIMETER WAVE PROPAGATION THROUGH RAIN

G. INTRODUCTION

The nonreciprocal nature of millimeter wave propagation through precipitation has received little attention in the literature. Nevertheless, in some applications the reciprocal and nonreciprocal properties of a communication system with precipitation along the propagation path are important. For example, the downlink signals on an earth-space communication link could be used in a polarization orthogonality restoration system [22]. The downlink effects on the signals must be the same as on the uplink (i.e. the medium must be reciprocal) in order to correctly apply adaptive cancellation to the uplink. Also reciprocity can play a role in millimeter wave experiments involving precipitation media.

In this part of the report we discuss those characteristics of a propagation medium which lead to nonreciprocal behavior and the signal parameters which they affect. A few simple examples for millimeter wave signals passing through rain are presented together with numerical results.

H. THEORY

Consider a millimeter wave signal propagating in the +z-direction with a depolarizing medium (such as precipitation) somewhere along the path. The output electric field components are given by

$$\begin{bmatrix} E_x \\ E_y \end{bmatrix} = [D] \begin{bmatrix} E_x^i \\ E_y^i \end{bmatrix} = \begin{bmatrix} D_{xx} & D_{xy} \\ D_{yx} & D_{yy} \end{bmatrix} \begin{bmatrix} E_x^i \\ E_y^i \end{bmatrix} \tag{18}$$

where E_x^i and E_y^i are the electric field components associated with the incident wave. The depolarization matrix [D] represents the change in the incident field due to the presence of the depolarizing medium; it is the identity matrix for an entirely free space path. There are various models available [24,25,5] for determining the complex-valued entries of [D] for precipitation media. However, for this investigation into nonreciprocal behavior, the general properties of [D] are of primary interest.

If the received signals on a dual polarized propagation link are the same upon interchange of the transmitter and receiver, the medium is said to be reciprocal. The well-known reciprocity theorem states that if a medium is linear and isotropic, but not necessarily homogeneous, it is reciprocal. But a precipitation medium such as rain is anisotropic since it contains oblate raindrops with scattering properties that depend upon the incident polarization. It is usually assumed that oblate raindrops are either equioriented or canted symmetrically. Then reciprocity still holds. But if the medium is also inhomogeneous along the propagation path with respect to canting angle, then the medium will be nonreciprocal.

To see this, consider a piecewise inhomogeneous path consisting of two cells, each of which is linear, homogeneous, and symmetrically anisotropic. The homogeneous condition for each cell permits uniform mixtures of various particle sizes and shapes. Let the depolarization matrices $[C_1]$ and $[C_2]$ represent the cell behavior in a manner similar to (18). Suppose an incident wave with components $E_x^{\,i}$ and $E_y^{\,i}$ enters cell 1 first and then cell 2, which we shall refer to as case a. Then

$$\begin{bmatrix} E_x^{\,a} \\ E_y^{\,a} \end{bmatrix} = [C_2][C_1] \begin{bmatrix} E_x^{\,i} \\ E_y^{\,i} \end{bmatrix} \tag{19}$$

The same input wave propagating in the reverse direction (case b) produces the following output field components

$$\begin{bmatrix} E_x^{\,b} \\ E_y^{\,b} \end{bmatrix} = [C_1][C_2] \begin{bmatrix} E_x^{\,i} \\ E_y^{\,i} \end{bmatrix} . \tag{20}$$

The overall depolarization matrices for the two cases are

$$[D^a] = [C_2][C_1] \quad \text{and} \quad [D^b] = [C_1][C_2] . \tag{21}$$

Performing the indicated matrix multiplications in (21) and comparing entires in the matrices $[D^a]$ and $[D^b]$ reveals that

$$D_{xx}^{\,a} = D_{xx}^{\,b} \quad , \quad D_{yy}^{\,a} = D_{yy}^{\,b} \quad , \tag{22a}$$

$$D_{xy}^{\,a} = D_{yx}^{\,b} \quad , \quad D_{yx}^{\,a} = D_{xy}^{\,b} \quad . \tag{22b}$$

This result is independent of the properties of the cells, except that each cell must have a symmetric matrix.

For the piecewise inhomogeneous medium to be reciprocal, the total path effects must be the same for the two propagation directions. Thus $[D^a] = [D^b]$, i.e. $[C_1]$ and $[C_2]$ must commute. Equating entries from the results of (21) gives, in addition to (22),

$$D_{xy}^{\ a} = D_{yx}^{\ a} \quad \text{and} \quad D_{xy}^{\ b} = D_{yx}^{\ b} \ . \tag{23}$$

Therefore, the depolarization matrix for the entire medium must be symmetric. This is a familiar result for two-port network scattering matrices.

If the total path depolarization matrix is not symmetric, in general signal attenuation and crosspolarization will not be reciprocal. Consider a precipitation path with two rain cells each with arbitrary but uniform rain rate and canting angle. This two cell medium is reciprocal, i.e. (23) is satisfied, if and only if [5]

$$\theta_2 - \theta_1 = n \frac{\pi}{2} \qquad n = 0,1 \tag{24}$$

where θ_1 and θ_2 are the canting angles for the oblate raindrops in the cells 1 and 2. Thus, nonreciprocity arises from discontinuities in the canting angles of the rain along the path, in particular when the principal drop axes are not aligned and do not differ by 90°. Equation (24) also holds for two cells each having a symmetric distribution of canting angles where θ_1 and θ_2 are now mean canting angles for the distributions.

The attenuation and cross polarization introduced by the medium are of interest for communication system calculations. These can be obtained by computing the components of the electric field intensity exiting the medium which are co- and cross-polarized to the incident electric field. For arbitrary incident polarization, attenuation and crosspolarization

ratio (CPR) are not reciprocal if the raindrops are canted differently along the propagation path. In most situations the effects on attenuation are negligible and, in fact, it can be shown that the attenuation is exactly reciprocal for linear input polarization. However, in certain situations CPR differences for opposite propagation directions can be significant.

I. EXAMPLES

As a simple example, consider a rain medium with two uniform cells of arbitrary rain rate and extent. Let cell 1 have all equioriented oblate raindrops aligned with their major axes horizontal. In cell 2 all drops are aligned but differently from those of cell 1. The incident polarization is vertical linear. Then the difference in CPR between forward and reverse propagation is

$$\Delta CPR(dB) = CPR^a(dB) - CPR^b(dB) = A_{H1}(dB) - A_{V1}(dB) \qquad (25)$$

where $A_{H1}(dB)$ and $A_{V1}(dB)$ are attenuations in dB of cell 1 for linear polarizations along the major and minor drop axes, respectively. [5] Note that this result is independent of the canting angle, length and rain rate of cell 2. For the case of a 2 km length of cell 1 along a path with a 40° elevation angle, the CPR difference of (25) is plotted in Fig. 11 for three frequencies using available differential attenuation values [23]. Note that the CPR difference increases with increasing rain rate.

Another example illustrates the effects of different canting angles in the two cell rain. Again the incident polarization is vertical linear, but the canting angles (of drop major axes relative to horizontal) of drops in cells 1 and 2 are θ_1 and θ_2. For this case, and for an identical rain rate and path length in both cells,

$$\Delta CPR(dB) = 20 \log \frac{|1 + g \cot \theta_1 \tan \theta_2|}{|g + \cot \theta_1 \tan \theta_2|} \qquad (26)$$

where $g = \exp[\alpha_H - \alpha_V + j(\beta_H - \beta_V)]L$ in which $\alpha_H - \alpha_V$ and $\beta_H - \beta_V$ are the differential attenuation and phase constants and L is path length of each

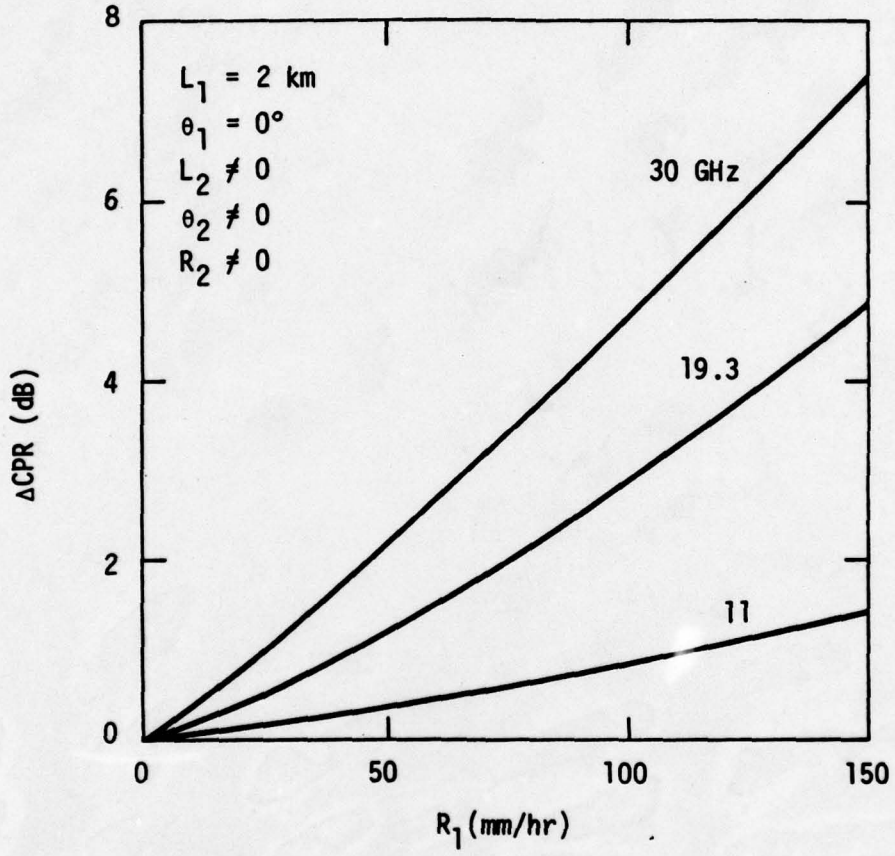

Figure 11. Difference in CPR for opposite directions of propagation through two rain cells as a function of rain rate in cell 1, which has a canting angle of 0° and a length of 2 km. Cell 2 has arbitrary, but nonzero, rain rate. canting angle, and length. The incident polarization is vertical linear and the path elevation angle is 40°.

cell. [5] The CPR for forward and reverse propagation are shown in Fig. 12 for 30 GHz, 20° elevation angle, cell lengths of 5 km, a rain rate of 25 mm/hr in both cells, θ_1 = 15°, and θ_2 variable. Note that ΔCPR(dB) = 0 for θ_2 = 15° when all drops are aligned when n = 0 in (24), and for θ_2 = 105° when n = 1 in (24). The CPR difference is also zero for θ_2 = 165° when $\theta_2 = \pi - \theta_1$ and the drops are symmetrically canted having a cancelling effect in this case.

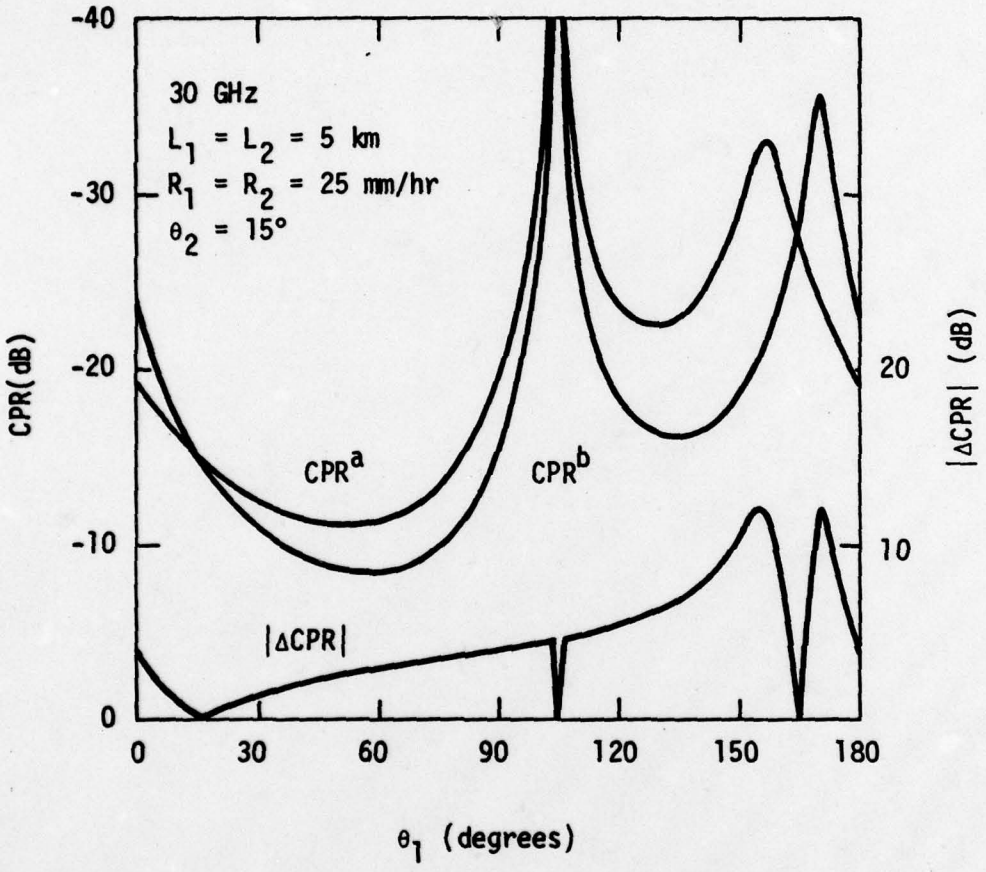

Figure 12. Crosspolarization ratio, CPR^a and CPR^b, for forward and reverse propagation and their difference, $|\Delta CPR|$, for two rain cells each of length 5 km, as a function of the canting angle of cell 1. The canting angle of cell 2 is 15°. The rain rate for both cells is 25 mm/hr. The frequency is 30 GHz, the elevation angle is 20° and the incident polarization is vertical linear.

J. CONCLUSIONS

Precipitation media with different canting angles along the propagation path are nonreciprocal. For the simple two rain cell examples presented noticeable CPR differences between forward and reverse propagation were shown to exist, especially for high frequencies and high rain rates. When data on canting angle differences in real rain or in mixtures of rain and ice media are available, the resulting impact on the nonreciprocal behavior can be calculated.

K. REFERENCES

22. R. W. Kreutel, D. F. DiFonzo, W. J. English, and R. W. Gruner, "Antenna technology for frequency reuse satellite communications," *Proc. of IEEE*, vol. 65, pp. 370-377, 1977.

23. T. Oguchi, and Y. Hosoya, "Scattering properties of oblate raindrops and cross polarization of radio waves due to rain (part II): calculations at microwave and millimeter wave regions," *J. of Radio Res. Labs* (Japan), vol. 29, pp. 191-259, 1974.

24. N. K. Uzunoglu, B. G. Evans, and A. R. Holt, "Scattering of electromagnetic radiation by precipitation particles and propagation characteristics of terrestrial and space communication systems," *Proc. IEE*, vol. 124, pp. 417-424, 1977.